BIOCHEMISTRY
including biophysical chemistry & molecular biology

Article

pubs.acs.org/biochemistry

The Linker of the Interferon Response Factor 3 Transcription Factor Is Not Unfolded

Hem Shukla,[†] Paulius Vaitiekunas,[†] Ananya K. Majumdar,[†] Anatoly I. Dragan,[†,‡] Emilios K. Dimitriadis,[§] Svetlana Kotova,[§] Colyn Crane-Robinson,*[,†,∥] and Peter L. Privalov[†]

[†]Department of Biology, Johns Hopkins University, Baltimore, Maryland 21218, United States

[‡]Institute of Fluorescence, University of Maryland, Baltimore, Maryland 21201, United States

[§]National Institutes of Health, Bethesda, Maryland 20892, United States

[∥]Biophysics Group, School of Biological Sciences, University of Portsmouth, Portsmouth, U.K.

ABSTRACT: Interferon response factor 3 (IRF-3) is a transcription factor that plays an essential role in controlling the synthesis of interferon-β (IFN-β) and is a protein consisting of two well-defined domains, the N-terminal DNA-binding and the C-terminal dimerization domains, connected by a 75-residue linker, supposedly unfolded. However, it was not clear whether in intact IRF-3 this linker segment of the chain, which carries the nuclear export signal and includes a region of high helical propensity, remains unfolded. This has been investigated using nuclear magnetic resonance by ligating the ^{15}N-labeled linker to the unlabeled N-terminal and C-terminal domains. It was found that, while the linker alone is indeed in a completely unfolded state, when ligated to the C-terminal domain it shows some ordering, and this ordering becomes much more pronounced when the linker is also ligated to the N-terminal domain. Thus, in intact IRF-3, the linker represents a folded structural domain; i.e., IRF-3 is a three-domain globular protein. Light scattering studies of wild-type IRF-3 showed that these three domains are tightly packed, and therefore, the dimer of IRF-3, which is formed upon phosphorylation of its C-terminal domains following virus invasion, must be a rather rigid and compact construction. One would then expect that binding of such a dimer to its tandem recognition sites PRDIII and PRDI, which are located on opposing faces of the IFN-β enhancer DNA, should result in deformation of the DNA. Analysis of the characteristics of binding of the monomeric and dimeric IRF-3 to the enhancer DNA indeed showed that formation of this complex requires considerable work for deformation of its components, most likely bending of the DNA. Such bending was confirmed by atomic force microscopy of dimeric IRF-3 bound to the PRDII−PRDI tandem recognition sites placed at the middle of a 300 bp DNA probe. Bending of DNA by IRF-3 must be significant in the assembly and function of the IFN-β enhancer.

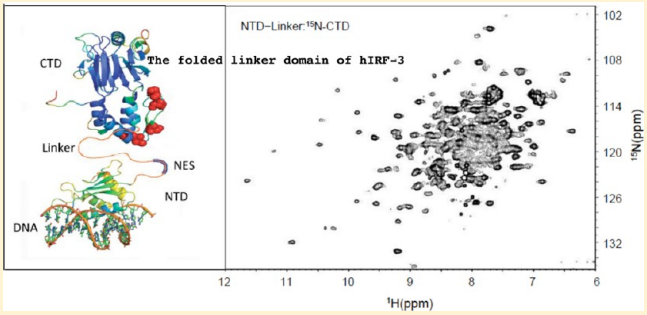

Interferon response factor 3 (IRF-3) is a transcription factor that plays an essential role in the organism's defense against pathogens: virus invasion triggers phosphorylation of the C-terminal domain of IRF-3, which leads to its dimerization and translocation as a dimer to the nucleus, where it binds by its two N-terminal domains to the PRDIII−PRDI tandem sites of the interferon-β (IFN-β) enhancer DNA (Figure 1a).[1−8] The C-terminal dimerization domain (CTD) of IRF-3 is connected to the DNA-binding N-terminal domain (NTD) by a 75-residue linker (Figure 1b), which was supposed to be unfolded.[7,9−14] When isolated, the linker indeed appears to be in a completely unfolded state, and it was found that the DNA binding ability of the N-terminal domain does not change upon activation and removal of the CTD.[15,16] It was thus natural to assume that the CTD holds the NTD on a long leash, which is needed to permit the two N-terminal domains of dimeric IRF-3 to bind to the PRDIII and PRDI sites that are rotationally displaced on the faces of the enhancer DNA (Figure 1c,d).

On the other hand, analysis of the sequence of the linker shows it has a very strong helical propensity in the central region and an unusually high content of regularly arranged proline residues (Figure 2). Moreover, it was found that this linker includes the nuclear export signal, (NES), which is responsible for the transportation of IRF-3 out of the nucleus, and deletions in the linker region result in autoimmune disease,[17] indicating that the linker plays some essential role in IRF-3 function. These considerations raised doubts about whether the 75-residue linker in IRF-3 is unfolded in the intact protein. However, if the linker is not unfolded, one would expect that binding of the two NTDs of the IRF-3 dimer to their tandem binding sites located on the opposite faces of the DNA should induce considerable deformation of the DNA, i.e.,

Received: February 26, 2012
Revised: July 19, 2012
Published: July 20, 2012

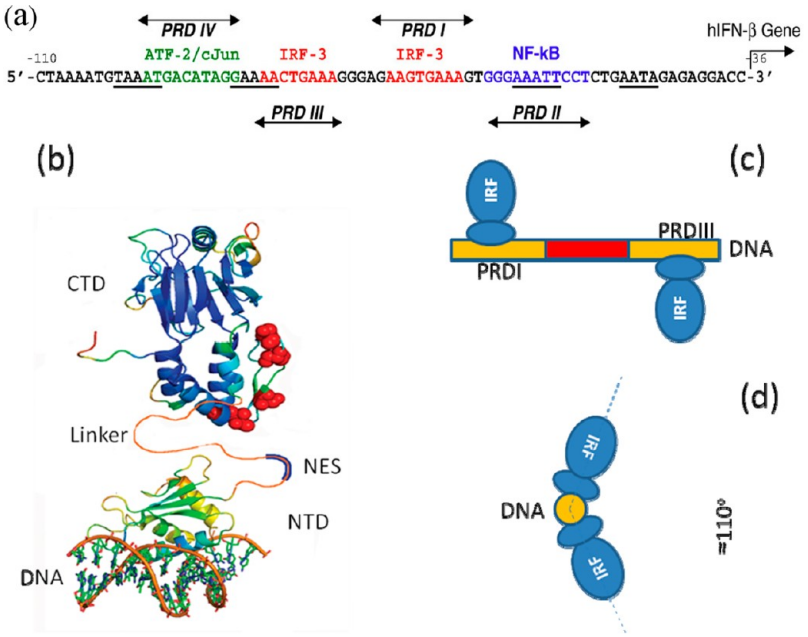

Figure 1. (a) IFN-β DNA. The PRDIII and PRDI target sites to which IRF-3 binds are colored red; the NF-kB site is colored blue, and the binding site for the bZIP pair is colored green. The underlined AT sequences are the proposed binding sites for HMGA1 molecules. (b) Structures of the DNA-binding N-terminal domain (NTD)[6] and the C-terminal dimerization domain (CTD) of IRF-3[7] connected by the 76-residue Pro-rich linker containing a nuclear export signal (NES), shown here as having a disordered conformation.[2,8] (c and d) Cartoons showing the relative position of two IRF proteins bound to the PRDI and PRDIII binding sites on the face of the IFN-β enhancer DNA in the B-form and the disposition to be expected if the linker domains are folded. Formation of an IRF-3 dimer mediated by the CTDs would seem to require considerable distortion of the DNA.

```
...-VGDFSQPTDSPDTNGGGSTSDTQEDILDELLGNMVLAPLPDPGPP-
   eecccccccccccttccccccchhhhhhhhhhhhhhhcccccccc

SLAVAPEPCPQPLRSPSLDNPTPFPNLGPSE-...
 ceeeccccccccccccccccccccccccccc
```

Figure 2. Sequence of the IRF-3 linker, residues 114−189 (first row) and its helical propensity (second row): h denotes a residue with strong helical propensity, t turn, e extended, and c random coil. The segment representing the NES has strong helical propensity and is shown in blue capital letters. It shows a regular arrangement of apolar residues typical for polypeptides that form helical coiled coils.[2,8] The expressed linker has an additional Cys-Trp dipeptide at its N-terminus.

its bending. The question is then whether bending of the DNA is required for assembly of the IFN-β enhanceosome.

The state of the linker is thus of principal importance for understanding the mechanism of IFN-β enhanceosome assembly and function. Crystallography has so far been unable to determine the state of the linker because both monomeric and dimeric IRF-3 have failed to crystallize. Hydrodynamic and optical measurements presented here suggest a folded state for the linker domain, and this has been definitively confirmed by nuclear magnetic resonance (NMR). Specific ^{15}N labeling of the linker was followed by its chemical ligation to unlabeled C- and N-terminal domains to generate an intact IRF-3 molecule showing strong dispersion of chemical shifts in the linker spectrum. Furthermore, atomic force microscopy (AMF) indicates bending of the DNA in complex with an IRF-3 dimer.

MATERIALS AND METHODS

Protein and Peptide Constructs. The wild-type IRF-3 monomer and its 5D phosphomimetic mutant that spontaneously forms a dimer were expressed and purified as described previously.[16] The 18-residue peptide Ac-WDTQEDIL-DELLGNMVLA-NH_2, representing a potentially helical segment of the IRF-3 linker, was chemically synthesized by Peptide 2.0 Inc.

Cloning and Expression of the ^{15}N-Labeled IRF-3 Linker. The linker domain of IRF-3 was amplified via polymerase chain reaction (PCR) from a clone of intact wild-type IRF-3 using 5′-GGAGGTGCTCTTCTGTTGGGTT-GGTGATTTTTCTCAACCT-3′ as the forward primer and 5′-GGAGGTTGCTCTTCATTTTCAGAAGGACCAAGA-TTAGG-3′ as the reverse primer. The forward primer includes an extra cysteine (TGT) for chemical ligation and an extra tryptophan (TGG) for concentration determination, and both include a SapI restriction site. The amplified product was purified, digested with SapI, and cloned into the pTWIN1 vector (New England Biolabs), generating the linker fused with Inteins I and II at the N- and C-terminal ends, respectively. This was transformed into BL-21 Gold DE-3 and a single colony grown in 5 mL of LB medium containing 100 μg/mL ampicillin overnight at 37 °C and tested for IPTG induction. Cells were then transferred into 2000 mL of LB medium and grown at 30 °C until the OD reached 0.5−0.7. After being pelleted at 6000 rpm for 10 min, cells were washed and repelleted in a 1× M9 salt solution (0.22 M KH_2PO_4, 0.48 M

dx.doi.org/10.1021/bi300260s | Biochemistry 2012, 51, 6320−6327

Na_2HPO_4, and 86 mM NaCl in 1000 mL). The cell pellet was resuspended in M9 minimal medium,[18] containing 10% (w/v) ^{15}N-labeled ammonium chloride (Cambridge Isotope Lab), transferred into 2000 mL of minimal medium, and grown for 20−30 min at 37 °C. IPTG (0.8 mM) was then added and the culture grown overnight at 18 °C, the cells being harvested at 8000 rpm for 15 min and resuspended in 25 mL of 20 mM phosphate buffer (pH 7.0), 1 mM EDTA, 500 mM NaCl, 0.1% Tween 20, 20 μM PMSF, and 1 mM DTT. Cells were disrupted by two passages in a French press at 10000 psi, and the crude lysate was centrifuged at 15000*g* for 20 min. The double-intein fusion protein was purified using a chitin column equilibrated with 20 mM phosphate buffer (pH 8.5), 500 mM NaCl, and 1 mM EDTA. The cell lysate was applied to the column at a flow rate of 0.5 mL/min at 4 °C, and the column was then washed with 10 volumes of 20 mM phosphate buffer (pH 8.5), 500 mM NaCl, 0.1% Tween 20, and 20 μM phenylmethanesulfonyl fluoride (PMSF) to remove unbound protein. The Intein I tag was removed by heating the column to room temperature overnight and then washing with 20 mM phosphate buffer (pH 7), 500 mM NaCl, 0.1% Tween 20, 20 μM PMSF, and 1 mM EDTA. Intein II was removed by equilibrating the column with 5 volumes of 20 mM phosphate buffer (pH 8.5), 500 mM NaCl, 1 mM EDTA, and 50 mM 2-mercaptoethanesulfonate, sodium salt (MESNA), overnight at 4 °C and the linker eluted with 20 mM HEPES buffer (pH 8.5), 500 mM NaCl, 1 mM EDTA, and 50 mM MESNA. The linker was purified on a Propac WCX-10 cation-exchange column and the eluted protein dialyzed into 20 mM phosphate buffer (pH 7.3), 500 mM NaCl, and 1 mM EDTA and stored at 4 °C for chemical ligation reactions.

Cloning and Expression of the C-Terminal Domain of IRF-3. The CTD was amplified via PCR from a clone of intact wild-type IRF-3 using 5′-GGAGGTTGCCTCTC-CAACTGTCCTCTTAAACGTCTTCTT-3′ as the forward primer and 5′-GGAGGTCTGCAGTTAAGATTCACCAG-GACCTTG-3′ as the reverse primer. An extra cysteine residue and a SapI restriction site were included in the forward primer, and a PstI site was introduced into the reverse primer. The amplified PCR product was cloned into the pTWIN1 vector and transformed into BL-21 Gold DE-3 *Escherichia coli* competent cells to express the CTD with a cysteine residue on its N-terminal end, essentially as described above. The Intein tag was removed from the fusion protein by on-column cleavage, flushing quickly with 3 volumes of 20 mM phosphate buffer (pH 7) containing 500 mM NaCl, 50 mM MESNA, and 1 mM EDTA. The flow was then stopped and the column heated to room temperature for overnight incubation. The carboxy-terminal domain was eluted with 20 mM phosphate buffer (pH 7) containing 500 mM NaCl and 1 mM EDTA in 1 mL fractions. Homogeneous purified fractions were pooled and stored at 4 °C.

Cloning and Expression of the N-Terminal Domain of IRF-3. The NTD was amplified via PCR from a clone of intact wild-type IRF-3 using 5′-GGAGGTCATATGATGGG-TACTCCTAAA-3′ as the forward primer and 5′-GGAGGTTGCTCTTCCGCAACCAGAATTAACAAATTC-3′ as the reverse primer. An NdeI site is included in the forward primer and a SapI site in the reverse primer. The amplified PCR product was cloned into the pTWIN1 vector to express a carboxy-terminal Intein II fusion protein with the NTD and a C-terminal CBD, essentially as described above. The fusion protein was purified and then the Intein tag removed by on-column cleavage, as described above. Finally, the N-terminal domain was eluted and dialyzed into 20 mM phosphate buffer (pH 7.3), 500 mM NaCl, and 1 mM EDTA and stored at 4 °C for further use.

Chemical Ligation of the ^{15}N-Labeled Linker with the CTD and NTD. The ^{15}N-labeled linker domain was first chemically ligated to the CTD by means of the latter's N-terminal cysteine residue and the carboxy-terminal thioester group of the expressed linker. The ligation was induced by 50 mM MESNA in 20 mM HEPES buffer, 200 mM NaCl, 100 mM DTT, and 1 mM EDTA (pH 7.3) at 4 °C. The initial trans-thioesterification reaction was followed by a spontaneous intramolecular S−N acyl shift to generate an amide bond at the ligation junction.[19,20] Subsequently, the cysteine residue present at the N-terminal end of the linker, now part of a linker−CTD fusion, was induced to react with the carboxy-terminal thioester of the NTD by treatment with MESNA as described above, leading to an intact IRF-3 molecule with only the linker containing ^{15}N. The integrity of the final product was checked by matrix-assisted laser desorption ionization mass spectrometry: a single peak at 47554 Da was observed. The calculated mass is 47611 Da, a difference of 0.1% and well within experimental error.

Synthesis of a 300 bp DNA Fragment Containing the IFN-β Enhancer Sequence. A 300 bp DNA fragment containing the centrally located 74 bp enhancer sequence was synthesized by Integrated DNA Technology. After digestion with EcoRI and SalI, the product was gel purified and ligated into the pIDTSMART cloning vector (IDT). This was transformed into DH5α competent cells and grown on LB plates containing 100 μg/mL ampicillin. Ten bacterial clones were picked and separately grown in 5 mL of LB containing 100 μg/mL ampicillin. The presence of the correct insert was verified by sequencing and an individual clone grown in 250 mL of LB medium containing 100 μg/mL ampicillin at 37 °C. The plasmid was purified using a QIAfilter Maxi kit (Qiagen, Inc.) and 10 μg digested with EcoRI and SalI to release the 300 bp insert, which was purified using a Qiaquick gel extraction kit (Qiagen, Inc.) and quantified photometrically.

Measurement of Two-Dimensional (2D) $^{1}H-^{15}N$ HSQC NMR Spectra. The $^{1}H-^{15}N$ HSQC spectra were acquired at 20 °C on a 600 MHz (^{1}H) Bruker Avance spectrometer equipped with a triple-resonance TCI cryoprobe. Parameters used for the ^{1}H and ^{15}N dimensions were as follows: spectral width, 18.3 ppm for ^{1}H and 28.0 ppm for ^{15}N; acquisition time, 60.0 ms for ^{1}H and 44.0 ms for ^{15}N; time domain data points (complex), 652 for ^{1}H and 77 for ^{15}N; number of scans/FIDs, 192; relaxation delay, 1.0 s. Water suppression was achieved using a flipback-watergate sequence,[21,22] and States−TPPI quadrature detection[23] was employed in the t_1 (^{15}N) dimension. Data were processed using nmrPipe.

Atomic Force Microscopy. The 300 bp DNA fragment and IRF-3-5D were mixed in a 1:2 molar ratio (25 nM:50 nM) in 10 mM phosphate buffer, 138 mM NaCl, and 2.7 mM KCl (pH 7.4) and incubated for 1 h at room temperature. Sample solutions (5 μL) were deposited on clean mica substrates (12 mm muscovite, grade V-1 mica disks), left to incubate for 10 min, and then gently rinsed with ∼0.5 mL of ultrapure, deionized water to remove salts and unattached molecules before being dried in a stream of argon. All imaging was performed under ambient conditions using a Multimode-Picoforce atomic force microscope equipped with a NS-V controller (Bruker Nano-Surfaces). Silicon probes (OTESPA,

Bruker Nano-Surfaces) with a nominal stiffness of 42 N/m and resonance frequencies of 300 kHz were used in the oscillating (tapping) mode. Images were acquired at ≈1 nm/pixel resolution. The mica surfaces had previously been modified by being incubated with a 0.17 mM solution of 1-(3-aminopropyl)silatrane (APS) in ultrapure water.[24] The modified mica surface possesses positive charges and is also hydrophobic. IRF-3-5D was imaged on freshly cleaved mica. Atomic force microscopy (AFM) images were preprocessed with the instrument software and then imported into NIH ImageJ for particle volume estimation.

Volumes were estimated by first thresholding the measured objects at half-height to minimize sample dilation caused by the finite probe size. The volumes of the thresholded particles were then estimated by summing the height values at every pixel within the particle base. The molecular mass of the particles was then computed by assuming a partial specific volume of 0.74 cm^3/g for the proteins and a 30% mass ratio of residual hydration water under ambient conditions. DNA lengths were measured by tracing the most probably maximal heights along the DNA contours.[25]

RESULTS AND DISCUSSION

Helicity of the Linker. The part of the IRF-3 linker having strong helical propensity (Figure 2) might play a role in forming a folded conformation. To test this possibility, the linker (with an extra Trp residue at its N-terminus for concentration determination) was investigated by CD. Whereas in buffer alone the spectrum of the isolated 75-residue linker is that expected for a random coil conformation (a negative minimum at 198 nm), upon addition of trifluoroethanol (TFE) there is clear evidence of helix formation with a transition centered at ~16% TFE (Figure 3). Inspection of the 17-residue sequence shows that the helix would be highly amphipathic, with acidic residues along one side and hydrophobics along the opposite face, the latter perhaps interacting with a hydrophobic patch on the NTD such as the four-stranded β-sheet,[26] thereby helping to hold together the two terminal domains.

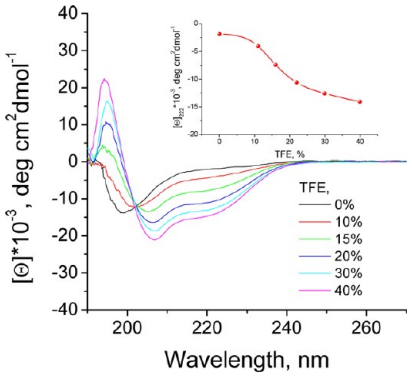

Figure 3. CD spectra of the polypeptide Ac-WDTQEDIL-DELLGNMVLA-NH_2 measured at different concentrations of trifluoroethanol (TFE). The inset shows the dependence of the mean residue ellipticity [Θ] at 222 nm upon the concentration of TFE.

Table 1. Hydrodynamic Radii (R_H) of the WT IRF-3 Monomer, the Dimeric 5D Mutant, and the Separate NTD

protein	no. of residues	R_H (nm)
WT	427	3.9
5D	854	4.9
NTD	113	2.3

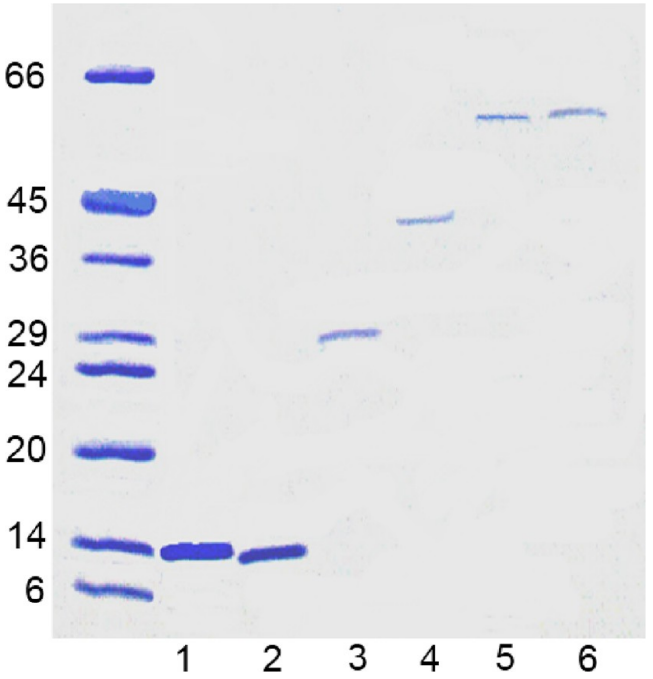

Figure 4. Electrophoresis (4 to 20% gradient polyacrylamide gel electrophoresis) of expressed IRF-3 constructs: lane 1, NTD; lane 2, ^{15}N-labeled linker; lane 3, CTD; lane 4, ^{15}N-labeled linker−CTD two-domain fusion; lane 5, NTD−N^{15}-labeled linker−CTD three-domain fusion; lane 6; wild-type IRF-3. The numbers for the marker lane are in kilodaltons.

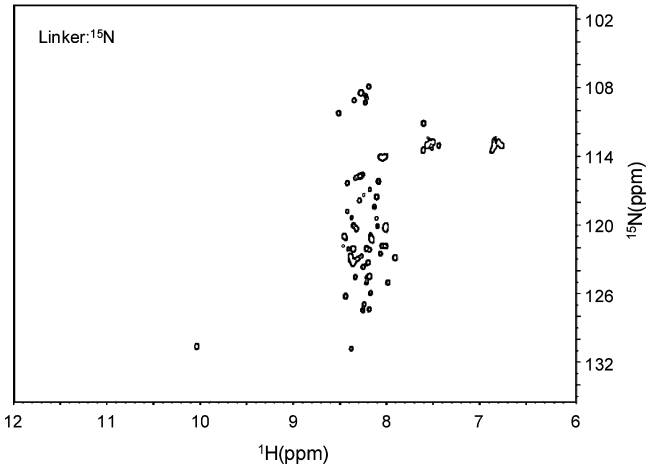

Figure 5. 2D $^1H-^{15}N$ HSQC spectrum of the ^{15}N-labeled linker in 20 mM phosphate buffer (pH 7.0) and 100 mM NaCl at 25 °C. The NMR spectra were recorded on a 600 MHz (^1H) Varian Inova spectrometer.

Compactness of IRF-3. An approach to deciding if IRF-3 is a compact globular protein, rather than an extended two-domain dumbbell species, is to measure hydrodynamic radii (R_H) by dynamic light scattering (Table 1). A disordered linker between the NTD and CTD would give rise to much greater apparent radii than a fully compact species. The IRF-3 WT monomer exhibited an R_H value that was 1.70 times that of the isolated NTD. If both species are considered as compact spheres of the same density, their relative radii would be (427/

dx.doi.org/10.1021/bi300260s | Biochemistry 2012, 51, 6320−6327

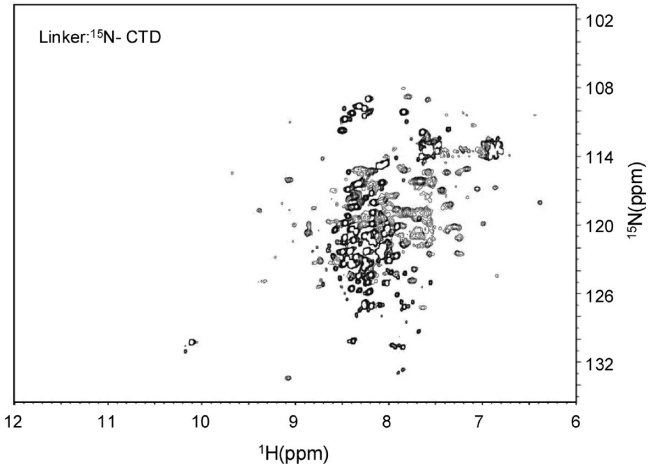

Figure 6. 2D $^{1}H-^{15}N$ HSQC spectrum of the ^{15}N-labeled linker ligated with the CTD in 20 mM phosphate buffer (pH 7.0) and 100 mM NaCl at 25 °C, showing that when bound to the CTD the linker partially adopts a folded conformation that is in slow exchange with an unstructured conformation.

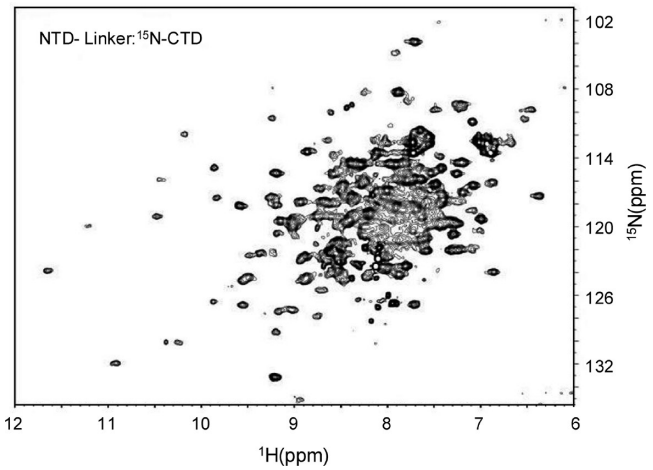

Figure 7. 2D $^{1}H-^{15}N$ HSQC spectrum of the ^{15}N-labeled linker ligated with both the NTD and CTD in 20 mM phosphate buffer (pH 7.0) and 100 mM NaCl at 25 °C showing that the linker adopts a predominantly folded structure.

113)$^{1/3}$, i.e., 1.56. The introduction of five phosphomimetic mutations to aspartate in the C-terminal dimerization domain of IRF-3 (designated IRF-3-5D) leads to its dimerization.[16] When the IRF-3 5D dimer is compared to the NTD in a like manner, their relative R_H values were found to be 2.1, whereas the predicted ratio is (854/113)$^{1/3}$, i.e., 1.96. These data imply that the IRF-3 monomer and dimer are both fully compact species.

State of the Linker. Folded and unfolded polypeptide chains are readily distinguished by their NMR spectra because the variety of chemical environments surrounding the individual amino acids in the folded form is manifested as a wide dispersion of chemical shift values. To observe a spectrum from the linker without interference (overlap) from the larger N-terminal and C-terminal domains of IRF-3, the protein chemical ligation procedure was adopted to construct an IRF-3 molecule having only the central linker domain labeled with ^{15}N, leaving the two flanking domains unlabeled (see Materials and Methods). First, the ^{15}N-labeled linker was expressed and

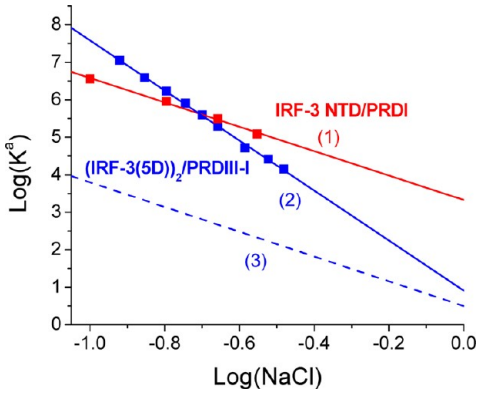

Figure 8. Dependencies of log(K_a) on log[NaCl] for association of the IRF-3 NTD (red line 1) with a 13 bp duplex representing the single site of PRDI and the IRF-3 5D dimer with a 26 bp duplex corresponding to the PRDI–PRDIII double site (blue line 2). The dotted line 3 shows the 5D binding data recalculated for one IRF molecule in the dimer, i.e., divided by 2. Because this is parallel to line 1, it follows that the dimer forms twice the number of salt links formed by the monomer. The slope of line 1 is −3.2, a value that corresponds to the formation of four or five salt links between DNA phosphate groups and basic residues of the NTD.[27] The crystal structure of the NTD bound to the enhancer DNA[26] shows four contacts in three of the four subunits bound.

then chemically ligated to the CTD to form an intermediate species, and this was subsequently ligated to the NTD to generate the complete IRF-3. After purification, all three species together with the separate CTD and NTD, and also wild-type IRF-3, were assessed for their size and chemical integrity by electrophoresis (Figure 4).

Figure 5 shows a $^{1}H-^{15}N$ HSQC spectrum of the isolated ^{15}N-labeled linker in 20 mM phosphate buffer and 100 mM NaCl (pH 7.3). Essentially all the resonance peaks are quite sharp and lie at a chemical shift of 8–8.5 ppm in the proton dimension, including the seven glycines clustered at a shift of ~110 ppm in the ^{15}N dimension. Bearing in mind the presence of 16 proline residues, we expect a total of 61 resonances from peptide groups. Resonances from nonpeptide groups are the pair of peaks at 6.8 and 7.5 ppm in the proton dimension deriving from the amide groups of the four asparagine and three glutamine groups, plus the single tryptophan peak at 10 ppm in the proton dimension. The lack of chemical shift dispersion in this spectrum indicates an essentially random coil, i.e., unfolded, conformation for the isolated linker at room temperature.

Figure 6 shows a $^{1}H-^{15}N$ HSQC spectrum of the intermediate species, i.e., the ^{15}N-labeled linker attached to the CTD, also in 20 mM phosphate buffer and 100 mM NaCl (pH 7.3). It is apparent that there is a significant increase in the dispersion of the chemical shifts, as compared with the spectrum of the isolated linker, indicating that some folding of the linker has occurred. However, the spectrum appears as the superposition of two subsets, one consisting of sharp peaks (those in the region of 8–8.5 ppm in the proton dimension) displaying poor dispersion and corresponding to a dynamic unstructured state, embedded on a background of broader but well-dispersed peaks corresponding to a folded, rigid conformation. Thus, the linker when bound to the CTD exhibits some propensity to form a folded conformation, which is in slow exchange with the unstructured conformation. This

dx.doi.org/10.1021/bi300260s | Biochemistry 2012, 51, 6320–6327

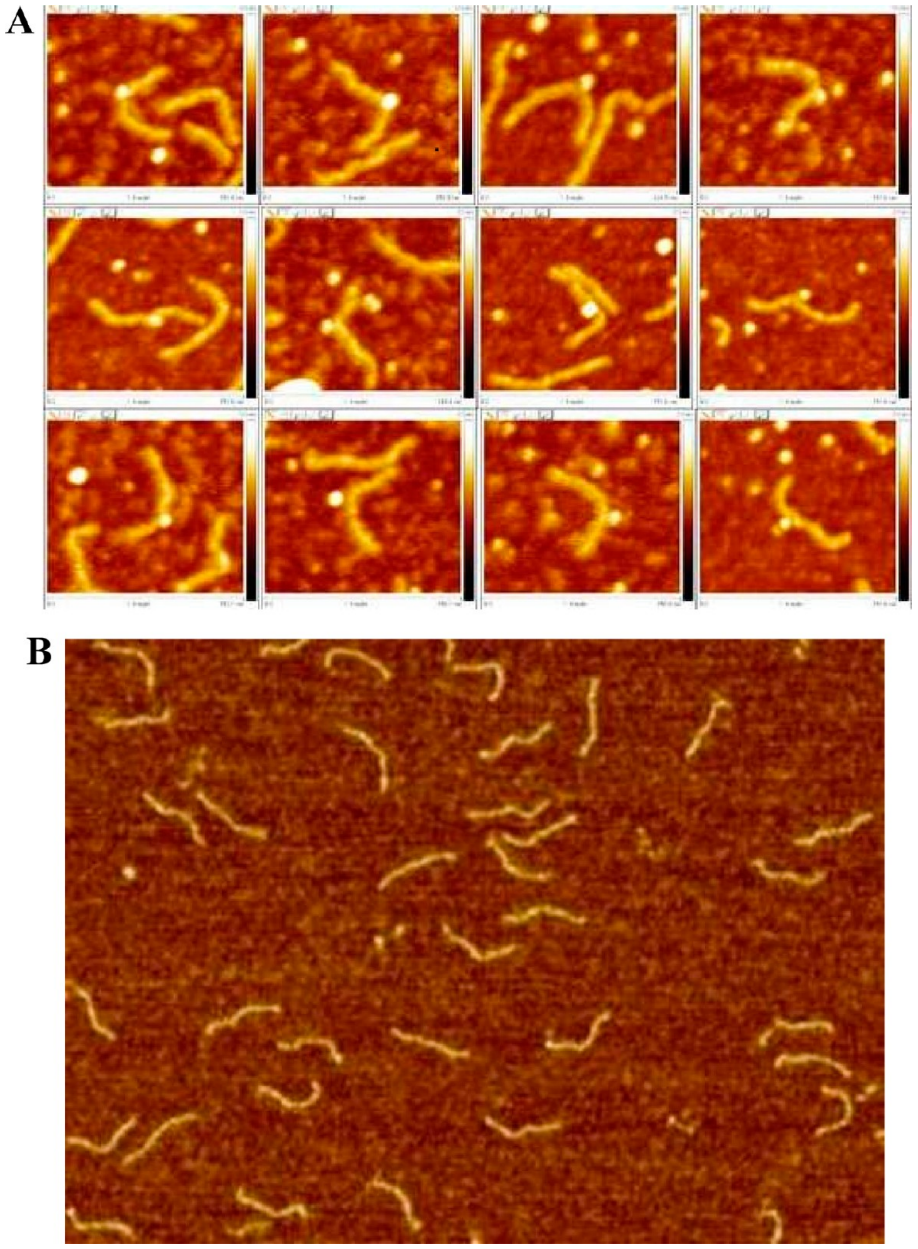

Figure 9. (A) AMF images of the complex of the 300 bp DNA, having the 74 bp IFN-β enhancer sequence in the middle, bound to the IRF-3 5D dimer showing that the protein bends the DNA considerably. (B) AFM images of the unbound 300 bp DNA.

explains the observation of more peaks than the 61 amide NH groups in the linker.

Figure 7 shows an equivalent spectrum for protons of the tridomain NTD−^{15}N linker−CTD construct, i.e., with the NTD added and corresponding to the wild-type IRF-3 monomer. It is clear that the dispersion of chemical shifts has increased very considerably. In contrast to the previous two constructs, the "strip" of resonances at 8−8.5 ppm in the proton dimension is no longer evident, nor is the cluster of seven glycines at a shift of ∼110 ppm in the ^{15}N dimension. This indicates that the linker has folded to a much greater extent upon further addition of the NTD to generate the whole IRF-3 monomer. The observation of more than 61 resonance peaks implies that this construct is not fully conformationally homogeneous: it appears that the folded conformation is in slow-exchange equilibrium with one or other conformations. The continuing presence of multiple peaks in the 8.0−8.5 ppm region suggests that some random coil segments might remain, but weak (i.e., minor component) peaks at the more extreme chemical shifts (10−12 ppm) imply an alternative folded conformation is present. Further experiments will be required to determine if this is an intrinsic property of the linker with functional consequences.

Two simple conclusions follow from these spectra. (a) The IRF-3 linker becomes largely folded upon incorporation between the two terminal domains, and (b) this is a property of the monomer, i.e., folding of the linker does not require dimerization of IRF-3.

Interaction of IRF-3 with the Target DNA. A compact ordered linker means that the dimeric CTD must effectively keep the two N-terminal domains on a short and fairly rigid leash, allowing them little freedom of movement. In that case, because the two PRDIII−PRDI binding sites are not on the same face of the DNA (Figure 1c,d), binding might result in

dx.doi.org/10.1021/bi300260s | *Biochemistry* 2012, 51, 6320−6327

some deformation of the complex, e.g., twisting and/or bending of the DNA. Additional evidence of distortion of the components upon formation of the complex is provided by a thermodynamic analysis of binding of IRF-3 to the IFN-β enhancer.

Using fluorescence anisotropy titrations to determine binding constants, a K_d value of 1.20 μM (i.e., ΔG = −33.1 kJ/mol) was observed for association of the IRF-3 5D dimer with a 13 bp target duplex, 5′-GAG**AAGTGAAA**GT-3′, corresponding to the PRDI site.[16] This represents binding of a single subunit, as evidenced by the fact that for binding of just the NTD to this 13 bp duplex K_d = 280 nM (i.e., ΔG = −36.7 kJ/mol), i.e., an only 10% difference. In contrast, for binding of the IRF-3 5D dimer to a 26 bp target duplex, 5′-GCG**AACTGAAA**GGGAG**AAGTGAAA**GT-3′, corresponding to the double PRDIII−PRDI sites, the measured K_d = 5.8 nM (i.e., ΔG = −46.1 kJ/mol). One might expect that the Gibbs energy of binding an IRF-3 dimer is twice that of a monomer, i.e., 2 × −33.1 = −66.2 kJ/mol, but in fact, it is only −46.1 kJ/mol; i.e., there is a deficit of 20 kJ/mol, representing free energy lost on binding the dimer. This must result from distortion, i.e., conformational changes, in the protein and/or DNA components.

To decide whether this free energy loss results from changes in electrostatic or nonelectrostatic interactions, the salt dependence of the binding constants was measured (see Figure 8) and plotted according to the relationship

$$\log(K^a) = \log(K^a_{nel}) - N \times \log[\text{salt}] \quad (1)$$

The slope of such plots, N, is a measure of the total number of electrostatic contacts between the protein and phosphate groups of the DNA,[27] and it is seen that the slope of the dimer plot (−6.5, corresponding to approximately nine salt links) is twice that for the binding of a monomer; i.e., the dimer forms twice the number of salt links formed by the monomer. There is therefore no difference in the electrostatic interactions of each monomer (salt links formed to DNA) in the dimer and the monomer conformations. The free energy deficit is therefore entirely nonelectrostatic in origin, and this must derive from conformational changes in the DNA or the protein.

IRF-3-Induced DNA Bending. DNA bending induced by the bound IRF-3 dimer was observed directly by an atomic force microscope using a 300 bp DNA with the entire 74 bp enhancer DNA (see Figure 1a) located in the center (see Materials and Methods). For this purpose, the phosphomimetic 5D mutant (S396D, S398D, S402D, and T405D) was expressed: this forms the dimer and interacts with the PRDIII−PRDI sites.[8,16] Images of the complex (Figure 9A) showed protein bound at the center of the DNA, and in many of the images (but not all), the DNA was bent at the point of protein binding. Such sharp bending was not seen in images of the free 300 bp probe (Figure 9B).

CONCLUSION

The linker of the monomer IRF-3 is folded, and the activated IRF-3 dimer represents a compact, rigid construct that, when bound to the IFN-β enhancer DNA, bends it considerably. Bending of the enhancer DNA by the activated IRF-3 must be significant for the assembly and function of the IFN-β enhanceosome.

AUTHOR INFORMATION

Corresponding Author

*Address: Portsmouth, PO1 2DT, UK. E-mail: colyn.crane-robinson@port.ac.uk. Telephone: +44-2392842520.

Notes

The authors declare no competing financial interest.

ACKNOWLEDGMENTS

The authors wish to acknowledge NIH grant 105365, entitled "The mechanism of Interferon Regulatory Factor (IRF) Activation".

REFERENCES

(1) Yoneyama, M., Suhara, W., Fukuhara, Y., et al. (1998) Direct triggering of the type I interferon system by virus infection; activation of a transcription factor complex containing IRF-3 and CBP/p300. *EMBO J. 17*, 1087−1095.

(2) Lin, R., Heylbroeck, C., Pitha, P. M., and Hiscott, J. (1998) Virus-dependent phosphorylation of the IRF-3 transcription factor regulates nuclear translocation, transactivation potential, and proteasome-mediated degradation. *Mol. Cell. Biol. 18*, 2986−2996.

(3) Hiscott, J., Pitha, P. M., Nguyen, H., et al. (1999) Triggering the interaction response: The role of IRF-3 transcription factor. *J. Interferon Cytokine Res. 19*, 1−13.

(4) Sato, M., Suemori, H., Hata, N., et al. (2000) Distinct and essential roles of transcription factors IRF-3 and IRF-7 in response to virus for IFN-α/β gene induction. *Immunity 13*, 539−548.

(5) Sakagushi, S., Negishi, H., Asaguri, M., et al. (2003) Essential role of IRF-3 in lipopolysaccharide-induced interferon-β gene expression and endotoxin shock. *Biochem. Biophys. Res. Commun. 306*, 860−866.

(6) Panne, D., Maniatis, T., and Harrison, S. C. (2004) Crystal structure of ATF-2/c-Jun and IRF-3 bound to the interferon-β enhancer. *EMBO J. 23*, 4384−4393.

(7) Qin, B. Y., Liu, C., Lam, S. S., Srinath, H., et al. (2003) Crystal structure of IRF-3 reveals mechanism of autoinhibition and virus-induced phosphoactivation. *Nat. Struct. Biol. 10*, 913−921.

(8) Lin, R., Mamane, Y., and Hiscott, J. (1999) Structural and functional analysis of interferon regulatory factor 3: Localization of the transactivation and autoinhibitory domains. *Mol. Cell. Biol. 19*, 2465−2474.

(9) Argos, P. (1990) An investigation of oligopeptides linking domains in protein tertiary structures and possible candidates for general gene fusion. *J. Mol. Biol. 211*, 943−958.

(10) Perham, R. N. (1991) Domains, Motifs, and Linkers in 2-Oxo Acid Dehydrogenase Multienzyme Complexes: A Paradigm in the Design of a Multifunctional Protein? *Biochemistry 30*, 8501−8512.

(11) Russell, G. C., and Guest, J. R. (1991) Sequence similarities within the family of dihydrolipoamide acetyl transferases and discovery of a previously unidentified fungal enzyme. *Biochim. Biophys. Acta 1076*, 225−232.

(12) Robinson, C. R., and Sauer, R. T. (1998) Optimizing the stability of single-chain proteins by linker length and composition mutagenesis. *Proc. Natl. Acad. Sci. U.S.A. 95*, 5929−5934.

(13) Dieckmann, R., Pavela-Vrancic, M., von Doehren, H., and Kleinkauf, H. (1999) Probing the domain structure and ligand-induced conformational changes by limited proteolysis of tyrocidine synthetase. *J. Mol. Biol. 288*, 129−140.

(14) George, R. A., and Heringa, J. (2002) An analysis of protein domain linkers: Their classification and role in protein folding. *Protein Eng. 15*, 871−879.

(15) Hargreaves, V. V., Makeyeva, E. N., Dragan, A. I., and Privalov, P. L. (2005) Stability and DNA binding ability of the DNA binding domains of interferon regulatory factors 1 and 3. *Biochemistry 44*, 14202−14209.

(16) Dragan, A. I., Hargreaves, V. V., Makeyeva, E. N., and Privalov, P. L. (2007) Mechanism of activation of the interferon regulator

factor-3: The role of C-terminal domain phosphorylation in IRF-3 dimerization and DNA binding. *Nucleic Acids Res. 35*, 3525−3534.
(17) Paun, A., Reinert, J. T., Jiang, Z., Medin, C., Balkhi, M. Y., Fitzgerald, K. A., and Pitha, P. M. (2008) Functional characterization of murine interferon regulatory factor 5 (IRF-5) and its role in the innate *antiviral* response. *J. Biol. Chem. 283*, 14295−14308.
(18) LeMaster, D. M., and Richards, F. M. (1982) Preparative-scale isolation of isotopically labeled amino acids. *Anal. Biochem. 122*, 238−247.
(19) Muir, T. W., Sondhi, D., and Cole, P. A. (1998) Expressed protein ligation: A general method for protein engineering. *Proc. Natl. Acad. Sci. U.S.A. 95*, 6705−6710.
(20) Muralidharan, V., and Muir, T. W. (2006) Protein ligation: An enabling technology for the biophysical analysis of proteins. *Nat. Methods 3*, 429−438.
(21) Piotto, M., Saudek, V., and Sklenar, V. (1992) Gradient-tailored excitation for single-quantum NMR-spectroscopy of aqueous solutions. *J. Biomol. NMR 2*, 661−665.
(22) Grzesiek, S., and Bax, A. (1993) The importance of not saturating water in protein NMR. Application to sensitivity enhancement and NOE measurements. *J. Am. Chem. Soc. 115*, 12593−12594.
(23) Marion, D., Ikura, M., Tschudin, R., and Bax, A. (1989) Improved solvent suppression in one- and two-dimensional NMR spectra by convolution of time domain data. *J. Magn. Reson. 85*, 393−399.
(24) Shlyakhtenko, L. S., Gall, A. A., Filonov, A., Cerovac, Z., Lushnikov, A., and Lyubchenko, Y. L. (2003) Silatrane-based surface chemistry for immobilization of DNA, protein-DNA complexes and other biological materials. *Ultramicroscopy 97*, 279−287.
(25) Cantor, C. R., and Schimmel, P. R. (1980) *Biophysical Chemistry: Part II: Techniques for the Study of Biological Structure and Function*, W. H. Freeman & Co., San Francisco.
(26) Escalante, C. R., Nistal-Villan, E., Shen, L., Garcia-Sastre, A., and Aggarwal, A. K. (2007) Structure of IRF-3 Bound to the PRDIII-I Regulatory Element of the Human Interferon-β Enhancer. *Mol. Cell 26*, 703−716.
(27) Privalov, P. L., Dragan, A. I., and Crane-Robinson, C. (2011) Interpreting protein/DNA interactions: Distinguishing specific from non-specific and electrostatic from non-electrostatic components. *Nucleic Acids Res. 39*, 2483−2491.